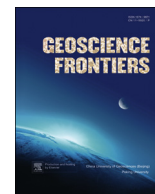Contents lists available at ScienceDirect

China University of Geosciences (Beijing)

# Geoscience Frontiers

journal homepage: www.elsevier.com/locate/gsf

Research paper

# Fault on-off versus strain rate and earthquakes energy

C. Doglioni [a,c,*], S. Barba [b], E. Carminati [a,c], F. Riguzzi [b]

[a] Dipartimento di Scienze della Terra, Università Sapienza, Roma, Italy
[b] Istituto Nazionale di Geofisica e Vulcanologia, Roma, Italy
[c] Istituto di Geologia Ambientale e Geoingegneria, CNR, Roma, Italy

## ABSTRACT

We propose that the brittle-ductile transition (BDT) controls the seismic cycle. In particular, the movements detected by space geodesy record the steady state deformation in the ductile lower crust, whereas the stick-slip behavior of the brittle upper crust is constrained by its larger friction. GPS data allow analyzing the strain rate along active plate boundaries. In all tectonic settings, we propose that earthquakes primarily occur along active fault segments characterized by relative minima of strain rate, segments which are locked or slowly creeping. We discuss regional examples where large earthquakes happened in areas of relative low strain rate. Regardless the tectonic style, the interseismic stress and strain pattern inverts during the coseismic stage. Where a dilated band formed during the interseismic stage, this will be shortened at the coseismic stage, and vice-versa what was previously shortened, it will be dilated. The interseismic energy accumulation and the coseismic expenditure rather depend on the tectonic setting (extensional, contractional, or strike-slip). The gravitational potential energy dominates along normal faults, whereas the elastic energy prevails for thrust earthquakes and performs work against the gravity force. The energy budget in strike-slip tectonic setting is also primarily due elastic energy. Therefore, precursors may be different as a function of the tectonic setting. In this model, with a given displacement, the magnitude of an earthquake results from the coseismic slip of the deformed volume above the BDT rather than only on the fault length, and it also depends on the fault kinematics.

© 2014, China University of Geosciences (Beijing) and Peking University. Production and hosting by Elsevier B.V. All rights reserved.

## 1. Introduction

An earthquake occurs when the volume close to a fault moves, the "fault on" stage. This coseismic stage is preceded by a long-lasting interseismic stage, called here as the "fault off" period. This evolution is commonly known as the seismic cycle (e.g., Thatcher and Rundle, 1979; Savage, 1983; Cattin and Avouac, 2000; Meade and Hager, 2005; Sieh et al., 2008). Faults are locked or unlocked depending on a number of parameters, including the presence of asperities and elasto-plastic instabilities (Kanamori and Anderson, 1975; Ruina, 1983; Hobbs and Ord, 1988; Marone, 1998).

In this paper, we consider the partitioning of strain between brittle and ductile structural levels as one of the mechanisms controlling the seismic cycle. The terms brittle and ductile could be substituted with Sibson's (1977) classification, where the elastic-frictional deformation dominates within the upper crust, and quasi-plastic deformation prevails in the lower, warmer crust. The terms brittle and ductile are used in the following for the sake of simplicity. The brittle behavior corresponds to frictional failure, whereas ductile deformation corresponds to thermally-activated creep. Faults and the related deeper shear zones evolve by different processes at different depths. A fault mylonite at depth corresponds to a cataclasite at shallower depth. At the transition between these two deformation mechanisms, viscous processes leave space to elastic-frictional processes at shallower depth. Although Sibson (1977) more precisely refer to the rheological processes, here we give emphasis to the simplicity of the fault activation model and we rely on a two-layer crust with a single brittle-ductile transition (BDT), mainly derived from Doglioni et al. (2011). Our model links the ongoing viscous deformation at depth with the fragile-brittle episodic behavior in the upper crust. We are clearly aware that this is an over-simplification since more than one

\* Corresponding author. Dipartimento di Scienze della Terra, Università Sapienza, Roma, Italy. Tel.: +39 06 49914549; fax: +39 06 4454 729.
*E-mail address:* carlo.doglioni@uniroma1.it (C. Doglioni).

BDT may occur in the crust as a function of the embedded lithologies. The results illustrate how the BDT focuses the energy loading in the overlying volume of rock during the interseismic stage. With the proposed rock deformation mechanics, the BDT and its depth control the energy accumulation, strain-rate distribution, and fault movement. In particular, we suggest that the strain rate gradients indicate stress accumulation. We compare the results of numerical models (Doglioni et al., 2011, 2013) with GPS data in a number of seismic crises in northern America, Chile, Italy, Taiwan and Turkey. Finally, a discussion on the different energy storage during the interseismic period is discussed as a function of the tectonic style.

## 2. Geological model of fault activation

The BDT represents the lower limit for most of the crustal seismicity worldwide (Scholz, 1990, and references therein), and it appears to have a relevant role in the description of the seismic cycle (Doglioni et al., 2011). The BDT separates the seismogenic elastic-frictional upper layer from the underlying quasi-plastic layer. In this scenario, stress in brittle upper crust builds up during the interseismic period until it ruptures seismically and deforms instantaneously reversing their relative motion along the conjugate bands formed above the BDT (Doglioni et al., 2011). We hypothesize an active fault crossing the entire crust exhibiting episodic locking-unlocking behavior in the brittle upper crust and a constant strain rate along the shear zone in the ductile lower crust (Fig. 1). At the BDT, the strain transfers from one zone to the other. During the interseismic period, the absence of dislocation in the brittle layer pairs with the continuous slip in the ductile layer and generates a stress gradient at the BDT. The stress gradient eventually dissipates, dislocating the brittle segment during the coseismic stage. In our model, the contrasting deformation style across the BDT acts as an "off" (locked or no displacement) and "on" (unlocked or active displacement) switch controlling the seismogenic behavior of the fault in the brittle layer.

### 2.1. Normal fault

In normal faulting, deep ductile deformation generates a dilation band nucleating from the BDT interface within the hangingwall volume, which is antithetic to the brittle, shallow, locked portion of the fault (Fig. 1). Although the lithostatic load increases with depth, the dilated band is inferred to expand at depth while approaching the BDT, and it should form for the differential motion between the steadily shearing lower ductile layer with respect to the locked upper brittle part of the hangingwall (Doglioni et al., 2011).

Dilatancy occurs in this tensional band, i.e., fractures and cracks form and open when rocks are stressed (e.g., Frank, 1965). The width of the dilated area (where fractures and cracks form) ranges from tens to hundreds of meters, up to the kilometric scale (Doglioni et al., 2011), depending on the mechanical properties of the rocks, which, in turn, vary as a function of the lithology and physical conditions (T, P, fluid pressure). During the interseismic period, the dilated volume may gradually expand to generate a band progressively weakened by fracturing, which allows (or depends on) fluid migration. Interseismic and preseismic fractures are expected to form parallel to the fault plane (and to $\sigma_2$), and with both antithetic and synthetic dip in the hangingwall volume above the BDT, particularly along the antithetic band. This weak band is predicted to form in the brittle layer where at the surface a strain rate gradient is observed. At the coseismic stage, the weak band could be activated as an antithetic normal fault (Fig. 1). For the L'Aquila 2009 event, the antithetic band activated as a conjugate normal fault may be located at the western border of the subsided area (as mapped by Atzori et al., 2009, by means of InSAR data),

where the strain rate was lower during the interseismic stage (Fig. 2). A second example is represented by the antithetic normal fault that slipped during the 40-s sub-event of the Irpinia 1980 earthquake in southern Italy (Pingue and De Natale, 1993). During the coseismic stage, the weight of the brittle hangingwall overcomes the strength of the weakened dilated band (Fig. 1). The triangle suddenly falls when the shear stress along the locked part of the fault overtakes the strength of the stretched band above the BDT. The hangingwall of the main fault instantaneously subsides closing the fractures in the dilated volume (Doglioni et al., 2011). The distribution of foreshocks and aftershocks of the L'Aquila earthquake agrees with this model in that foreshocks concentrated primarily along the dilated area above the BDT. The aftershocks (Chiarabba et al., 2009; Di Luccio et al., 2010) were rather well aligned along the activated upper segment of the normal fault and within the fallen hangingwall.

A field example of an outcropping paleo-BDT is the Permo-Liassic Lugano normal fault in the southern Alps, Italy (Bernoulli, 1964). The Alpine shortening exhumed such a fault, which can be analyzed in its different ductile and brittle portions. Metamorphism and shear is documented in the ductile deeper section at a paleodepth of 8—10 km (Bertotti et al., 1993) whereas several cracks occur in the brittle shallower part of the listric fault. Nuchter and Stockhert (2008) described cracks and veins, located close to the BDT. They proposed their generation during the coseismic stage. We wonder whether this relevant observation could fit the generation of veins also during the interseismic period, given the constraint that the overburden does not change significantly during vein formation. If this were the case, the veins would represent an exhumed analog of the dilated band forming during the interseismic stage at depth above the BDT, conjugate to the normal fault.

### 2.2. Thrust fault

Unlike the normal fault case, the hangingwall above the BDT of a thrust fault is compressed during the interseismic stage, accumulating elastic energy, and dilates at the coseismic stage, dissipating the energy stored (Fig. 1). In the Tohoku-Oki 2011 earthquake, the stress change suggests an active slip of several tens of meters along the plate interface during the coseismic fault weakening, a nearly total stress drop (Lin et al., 2013). The capacity to accumulate this energy depends on the rheological properties of the hangingwall. During the coseismic stage, elastic rebound is expected to generate uplift of the hangingwall above the brittle segment of the thrust fault and internal subsidence above the BDT, where some dilatancy is predicted to occur instantaneously in the area/volume previously overcompressed during the interseismic stage (Fig. 1). This model is consistent with the data and model presented by Burrato et al. (2003) for fault-propagation folding. A similar behavior was detected during the great 2004 Sumatra earthquake (Meltzner et al., 2006).

At the scale of an orogen, a similar evolution can be predicted. Along subduction zones, the slab hinge can either migrate toward or away from a reference point pinned on the upper plate (Doglioni et al., 2007). Along the Taiwan, Andean, Sumatra and Cascadia subduction zones, the hinge migrates towards the upper plate (i.e. eastward or northeastward), and the associated orogens undergo compression while the plate is moving westward or southwestward relative to the lower plate (Fig. 3). In these subduction zones, the convergence rate is accommodated partially by the subduction, and partially by upper plate shortening (Fig. 3). For example, the hinge of the Andean subduction zone is converging toward the South American upper plate (e.g., Doglioni et al., 2007). During the interseismic period, the steady movement of the GPS sites can be inferred as the superficial record of ductile deformation in the lower crust. Shortening is accommodated by stationary or steady
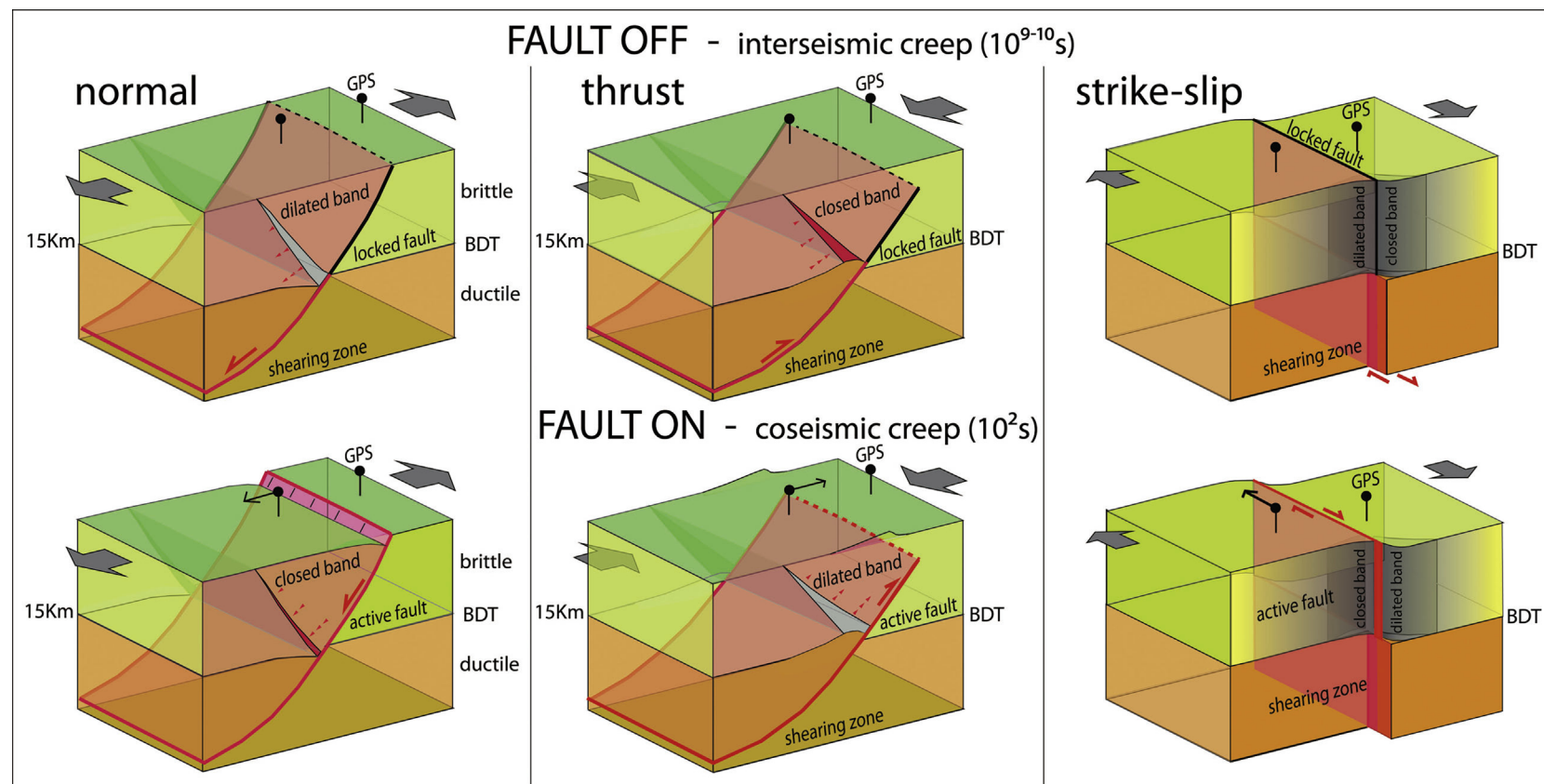
**Figure 1.** Geological model of fault on-off in the three main tectonic settings. During the interseismic period (fault off), the brittle-ductile transition (BDT) separates the elastic-frictional (brittle) upper crust, where the faults are almost locked, from their related deeper shear zones, which are instead constantly creeping in the quasi-plastic (ductile) lower crust. GPS sites at the surface show no motion between the two walls of the faults (upper figures). The upper crust above the BDT suffers dilation in the normal fault case, shortening in the thrust fault case, and two opposite bands of dilation and shortening in the strike-slip fault. During the coseismic stage (fault on), the faults of the brittle upper crust are activated, and the conjugate bands above the BDT experience opposite kinematics, i.e., the dilated volume is compressed, and the compressed volume is dilated. The bands that formed during the interseismic stage above the BDT at a high angle relative to the main fault, they may evolve into conjugate faults.
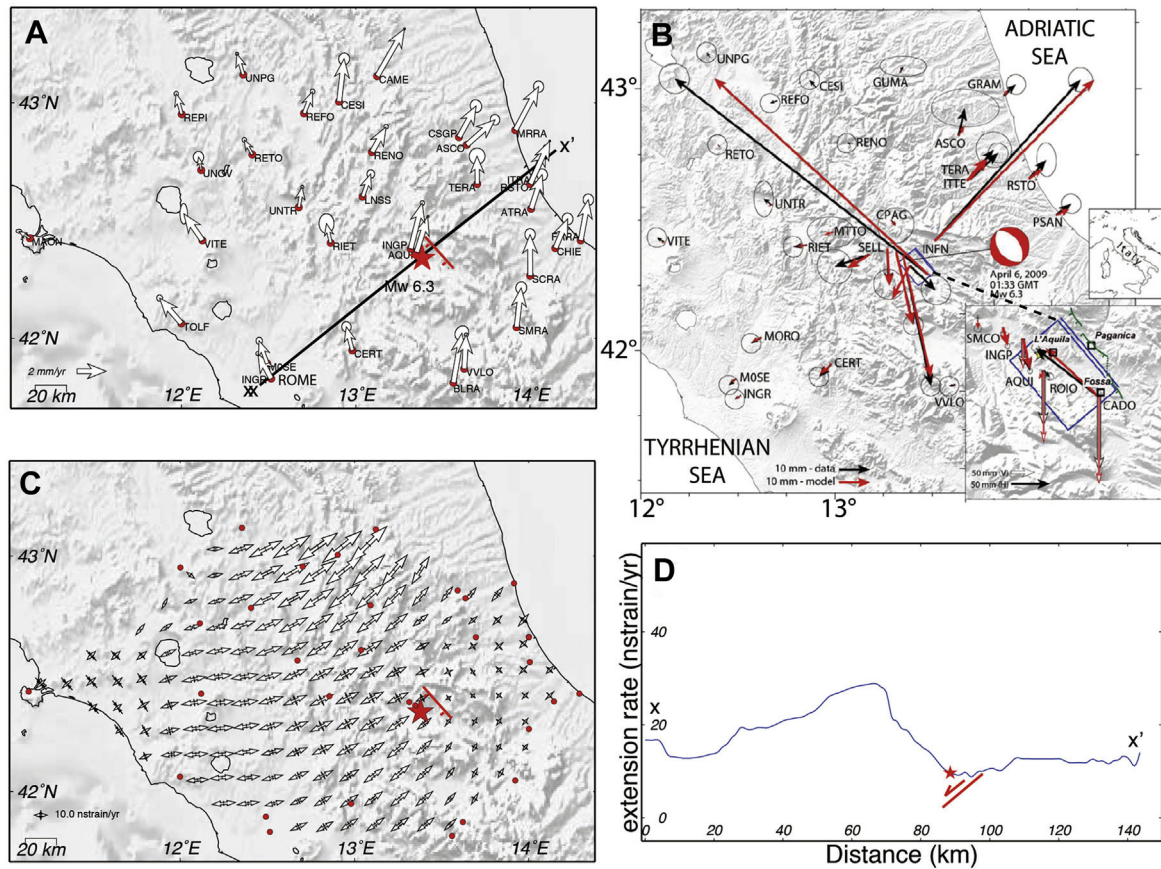
**Figure 2.** A: GPS interseismic velocity field in central Italy and the L'Aquila area relative to the stable Eurasia; the line indicates the trace of Section D, depicting the strain rate variation. Panel B displays the coseismic displacements (Anzidei et al., 2009); Panel C illustrates the strain rate principal axes on a regular grid based on the interseismic velocities based on the data before the 6th April, 2009, *M* 6.3 event. The fault nucleated in an area of low interseismic strain rate (Doglioni et al., 2011). The higher strain rate to the north is interpreted as related to the postseismic relaxation of the 1997–1998 Umbria-Marche seismic sequence, where the faults did not return yet to a locked condition. The red line represents the main activated fault.

state shear in the lower ductile crust where metamorphism takes place, and the faults in the shallower brittle crust are primarily locked. Elastic energy accumulates as the hangingwall becomes compressed. During the coseismic stages, the abrupt motion of the brittle portion of the crust is recorded by GPS coseismic displacement with an opposite versus with respect to the steady-state regime. The brittle portions of the fault move suddenly backward westward or southwestward with respect to the upper plate, i.e., towards the lower plate, similar to a previously compressed spring (Fig. 3). This simple model explains the GPS records of the seismic cycles and non-volcanic tremors along subduction zones such as Cascadia, Sumatra and the Andes. These subduction zones display similar evolution with an interseismic shortening between the GPS sites in the accretionary prism and the fixed upper plate, suddenly reversing toward the lower plate during the coseismic relaxation as proposed in Fig. 3. To support this model see the data by Dragert et al. (2001); Moreno et al. (2010); Prawirodirdjo et al. (2010). The observed coseismic vertical displacements show uplift and subsidence respectively west and east of the epicenter (Fig. 1), as shown in the thrust model of Fig. 1 above the coseismic dilation of the interseismically compressed band. For example, subsidence was also observed east of the Maule 2010 event (Fig. 4B).

### 2.3. Strike-slip fault

Assuming a simple strike-slip fault, subvertical and planar (without undulations, transtension or transpression) and cross-

cutting the entire crust, the two sides of the fault creep uniformly along the whole fault below the BDT at a rate similar to the rate of motion between the two plates. Therefore, in the ductile lower crust, we assume a stationary displacement rate along a ductile shear zone, but in the brittle upper crust, the fault creeps (partly or entirely unlocked) or does not slip (locked), as modeled in Fig. 1. Regional instances of strike-slip faults with both locked and unlocked segments have been described, e.g. along the San Andreas, the Dead Sea and the North Anatolia faults. For example, the cumulative offset along the Dead Sea Fault indicates episodic movements alternated with hundreds of years of rest in a locked condition (Klinger et al., 2000). The San Andreas Fault contains some segments of aseismic creep and other segments where the fault is practically locked (Rosen et al., 1998). The unlocked segments of the San Andreas Fault are thought to be lithologically controlled, given that they contain low-friction shale (Schleicher et al., 2010). The deep ductile creep along the main strike-slip faults is, however, proven by the motion of the GPS sites, regardless the single fault is locked or unlocked in the brittle upper part.

A model rather similar to that of Fig. 1 was proposed for the San Andreas Fault by Savage and Burford (1973) who subdivided the fault into two end members of tectonic behavior, i.e. the locked-fault model and the rigid-block model. In the locked fault model, the upper crust is not moving, whereas the motion occurs in the lower crust. In the rigid-block model, the entire crust moves apart along the fault.

If the brittle portion of a fault is locked, and the lower crust creeps slowly between the two walls, a decoupling (i.e., a
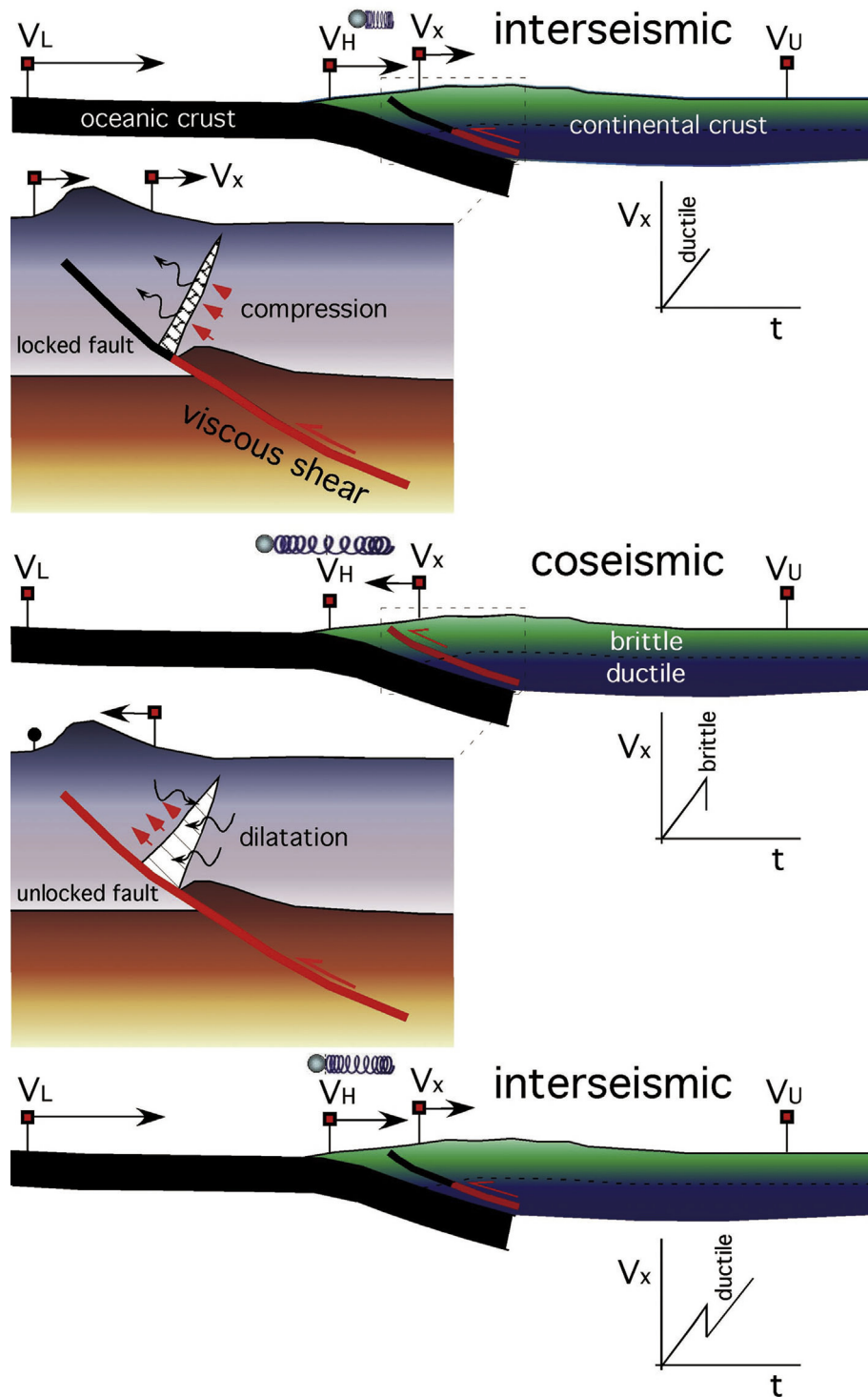
**Figure 3.** During the interseismic period, the orogen undergoes compression. The shortening is accommodated at depth by stationary shear in the lower ductile crust, although the upper crust faults are primarily locked. During the coseismic stage (middle panel), the brittle part of the fault suddenly moves backward with respect to the fixed upper plate, like a previously compressed spring. This model applies to the GPS record along the Cascadia and Sumatra seismic cycles. $V_L$, rate of motion of the lower plate; $V_H$, rate of motion of the subduction hinge; Vx, rate of motion of a reference point anchored to the brittle layer; $V_U$, fixed point on the upper plate. During the coseismic stage, Vx rebounds instantaneously in the direction opposite that during the interseismic period. The cumulative upper plate-directed shift of the reference (x) is characterized by interseismic periods of convergence and shortening toward the upper plate whereas the coseismic stage has an opposed rebound toward the lower plate.

discontinuity in the displacement rate) should occur at the BDT (Fig. 1). If the brittle portion of the fault is moving, the two brittle and ductile layers may be considered to be coupled (i.e., moving together without relative motion) or at least partially coupled. The "coupled" and "decoupled" terms in this manuscript refer strictly to

the continuity of displacement or the displacement rate across the BDT (Fig. 2 of Doglioni et al., 2013). In seismological parlance, however, coupling refers to the proportion of the total displacement accommodated by coseismic motion. At the tip lines of the BDT separating the coupled and decoupled upper brittle and lower
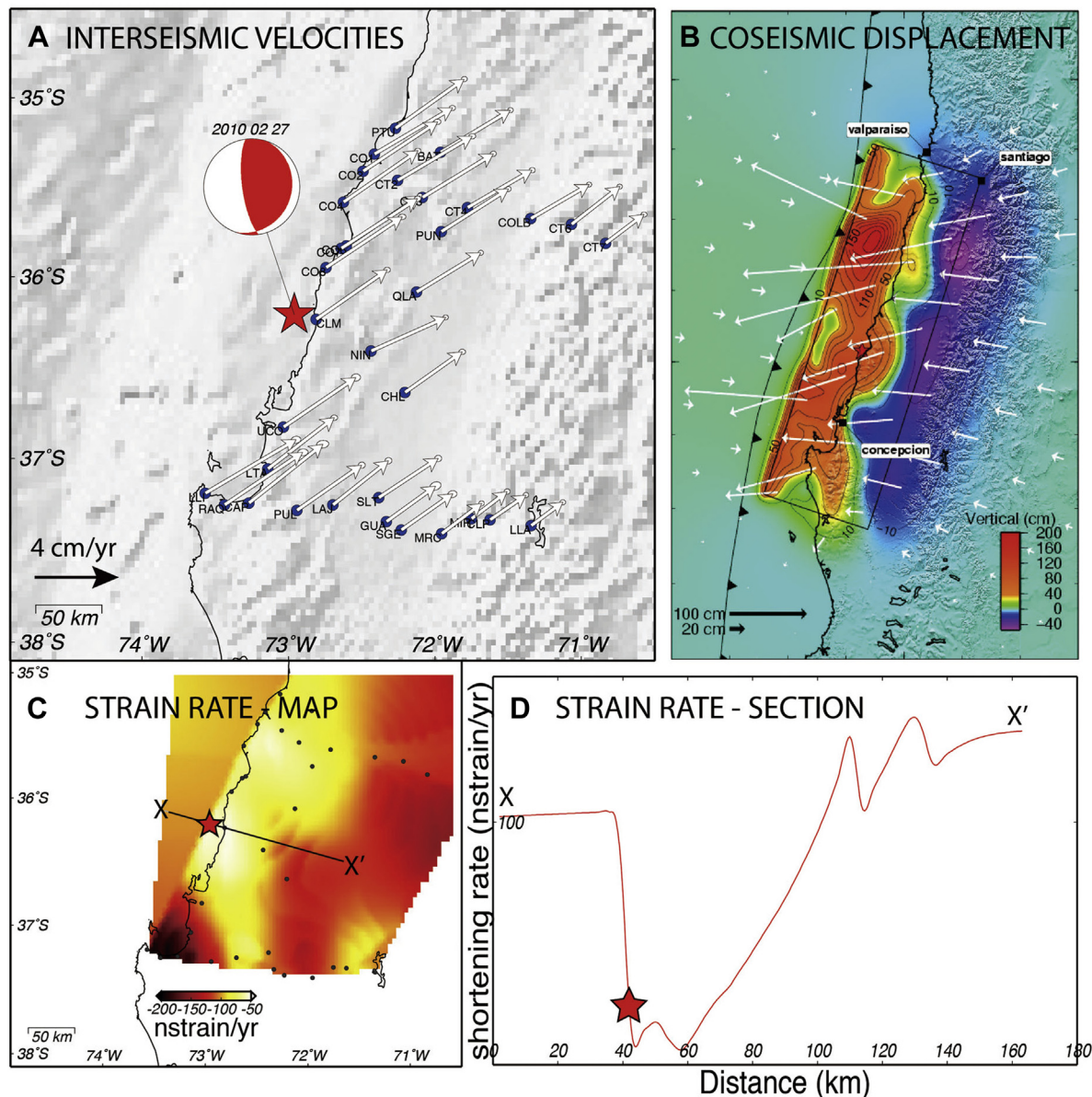
**Figure 4.** A: Map showing the interseismic rates of velocities near the Maule $M_w$ 8.8, February 27, 2010, Chile earthquake (data after Brooks et al., 2010; Moreno et al., 2010). During the interseismic stage, ENE-directed shortening toward the South America upper plate occurred. The shortening decreased towards the continental interior. B: The coseismic displacements during the Maule earthquake (after Sladen, 2010) are directed in the opposite (westerly) direction. This evolution reflects east-directed shortening and steady-state creep in the ductile crust during the interseismic period. The coseismic opposite direction rather indicates the west-directed elastic rebound of the brittle locked upper crust. The figure also depicts the surface deformation predicted by the slip model. The vertical component of displacement is shown by the color scale: red = uplift, blue = subsidence (after Sladen, 2010). The star indicates the epicenter of the mainshock. During the coseismic stage, the frontal part of the thrust undergoes uplift whereas the rear part subsides. C: Map of the strain rate with location of the epicenter. D: Trace of the strain rate section. Note that the event occurred in an area of high strain gradient in the segment of low strain rate. The strain rate offshore west of Chile is unconstrained due to the lack of GPS sites. However, the Maule earthquake generated in an area of relative interseismic lower strain rate, moving along strike (SSW–NNW) or dip (E–W) of the activated thrust.

ductile crust, two subvertical bands or aureoles should form: one dilational and the other contractional (Fig. 1). At the Earth's surface, the two bands develop at the tips of the locked segment of the strike-slip fault that corresponds to the portions of the crust decoupled at the BDT at depth (Fig. 1). At the tip lines, the brittle crust should slightly rotate and deform elastically. In the regions immediate to the fault tip, there should be significant stress shadows late in the interseismic period at the BDT, due to the adjacent locked fault as demonstrated by Hetland et al. (2010). The coseismic deformation at the tips of strike-slip faults is described by standard dislocation models (Okada, 1992; Feigl and Thatcher, 2006). The coseismic deformation at the tips of an activated fault

was captured after the Landers (1992) earthquake in California in an InSAR image (Massonnet et al., 1993).

Unlike normal and thrust faults, the motion along a strike-slip fault occurs parallel to an equipotential surface. In normal and thrust faulting, the antithetic band develops parallelly to $\sigma_2$, which is horizontal. In the strike-slip setting, $\sigma_2$ is vertical but parallel to the two strongly deforming bands.

## 3. Strain rate and regional examples

In extensional, contractional and strike-slip tectonic settings, the fault segments more likely to cause earthquakes present a

relatively low geodetic strain rate prior to seismic events with respect to the surroundings (Doglioni et al., 2011; Riguzzi et al., 2012, 2013). Savage and Prescott (1978) summarized how the slip across active faults increases after an earthquake in the earlier part of the seismic cycle, whereas it decreases toward the end of it. Analyzing the seismicity of Italy and the geodetic strain rate pattern, Riguzzi et al. (2012, 2013) showed that larger earthquakes occurred in areas of lower strain rate. Thus, strain rate mapping from interseismic GPS velocities (Devoti et al., 2008, 2011) may constitute an indicator of future occurrence of seismic events in tectonically active regions. In this study, we examine areas of well defined extensional, contractional and strike-slip styles and analyze both the geodetic interseismic velocity fields and the coseismic displacements of a few large-magnitude earthquakes.

We have estimated the strain rate from the interseismic GPS velocities, by a distance-weighted approach, computed using all stations on a regularly spaced grid applying a distance-weighting algorithm (Shen et al., 1996, 2007). This approach smoothes the strain rate, concealing the strain rate gradients and the behavior of single tectonic structures; nevertheless this interpolation allows recovering the strain rate from sparse data.

In this paragraph, we describe few different regional examples for each tectonic setting. The sections run parallel to the slip of the fault (i.e., down dip for normal and reverse faults, and along strike for the wrench fault).

As an example of normal faulting earthquake, we discuss the 2009 L'Aquila (Italy) event in the central Apennines (Fig. 2). Normal faulting dominates the upper crustal seismicity located along the

Apennines (Chiarabba et al., 2005), whereas a westerly-directed subducting slab affects the deeper events. The lower crust is seismically rather silent, suggesting a ductile rheology (Carafa and Barba, 2011). On April 6, 2009, a $M_w$ 6.3 earthquake occurred close to the city of L'Aquila (e.g., Chiarabba et al., 2009). The aftershock distribution evidences a composite NW–SE-trending extensional structure about 40 km long, typical for normal faults in the area (Vezzani and Ghisetti, 1998; EMERGEO Working Group, 2010; Galli et al., 2010) and composed of three main segments. The mainshock fractured the longest fault segment, nucleating at a depth of approximately 10 km. The propagation of the rupture and the aftershocks migrated upward from 10 to about 2 km, and consistently with the predictions of the normal fault model of Carminati et al. (2004). The seismogenic fault dips approximately 43–47° to the SW (Chiarabba et al., 2009). The rocks involved in the seismicity form a triangular prism of approximately 3000 km³. This crustal block moved down during the earthquake, rupturing at the mainshock and slowly collapsing in the following weeks and months until reaching a more stable condition. The maximum horizontal and vertical coseismic surface displacements detected at GPS stations were $10.4 \pm 0.5$ cm and $-15.6 \pm 1.6$ cm, respectively (Anzidei et al., 2009). The GPS between L'Aquila (AQUI) and Rome (INGR) indicated an interseismic extension rate of 2.5 mm/yr (Devoti et al., 2008; Anzidei et al., 2009; Devoti et al., 2011). In this paper, we considered such extension released along the ductile, unlocked portion of the fault. The surface expression of the pre-earthquake maximum strain-rate gradient was located to the west of the hypocenter of the April 6 mainshock; above the
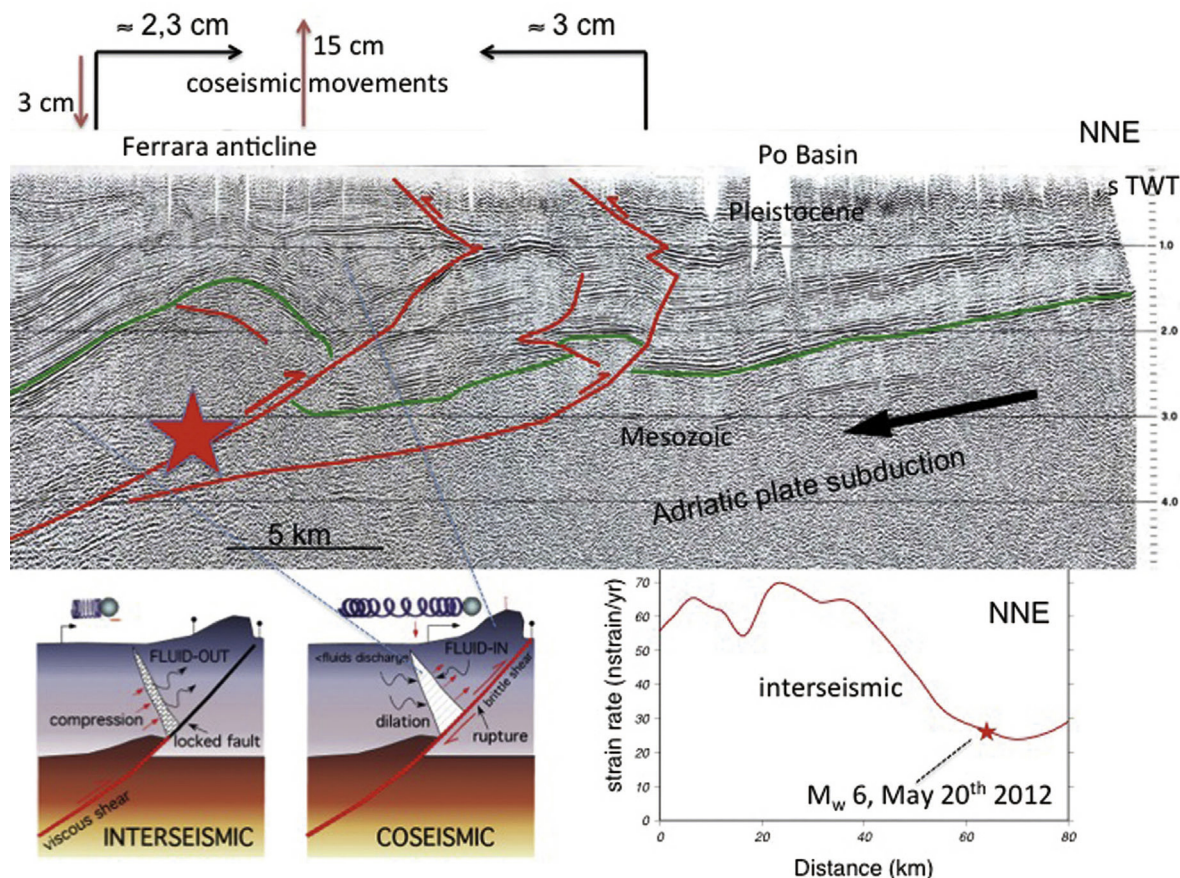


**Figure 5.** Interpretation of the main thrusts at the front of the Apennines accretionary wedge buried beneath the Po Basin in northern Italy, where May 20th 2012 a $M_w$ 6 thrust-related earthquake (red stars) occurred in the Emilia region. Note the shallow triangle zones in the upper parts of the thrusts. The epicenter was located in an area of relative lower strain rate (section in the right lower panel, expanded to the SSW of the seismic section). Another event struck the area few km to the south May 29th. Original seismic section from Pieri (1983).

easternmost normal faults, including the 2009 earthquake faults, the strain rate was at a minimum (Fig. 2). Assuming that the stretching rate was almost constant since 1703 when the last large earthquake hit the area, one can estimate approximately 75 cm of dilation between the locked and unlocked segments of the fault. This dilation is likely distributed over a wider section (tens to hundreds of meters). The L'Aquila April 6, 2009 earthquake generated a maximum coseismic slip of about 80 cm on the fault plane (Anzidei et al., 2009; Chiarabba et al., 2009). The volume of the upper crust that experienced extension during the interseismic stage should have been nearly closed during the coseismic stage. The epicentral area of the L'Aquila earthquake was characterized during the interseismic stage, by a pre-earthquake low strain rate (Riguzzi et al., 2012). In fact, the stronger shaking occurred in an area of low interseismic strain rate, close to a high gradient of interseismic strain rate (Fig. 2).

The Maule (Chile) earthquake, which occurred in the Andean thrust belt, provides an example for a compressive setting (Fig. 4). On February 27, 2010, a $M_w$ 8.8 thrust-related earthquake occurred at Maule in central Chile. The rupture initiated at the depth of approximately 32 km (Delouis et al., 2010) along a NNE-trending, 19° ESE-dipping thrust. The rupture propagated approximately 50-km down-dip in agreement with the lower limit of the locked zone inferred by Ruegg et al. (2009) from preseismic GPS data. The interseismic period all over the Andes is characterized by displacement of GPS sites towards the continental interior (e.g., Liu et al., 2000; Moreno et al., 2010), indicating shortening of the orogen at rates of 30–40 mm/yr eastward (Fig. 5), decreasing to zero at

the front of the retrobelt. This is consistent with the subduction hinge migration toward the upper plate, and the partitioning of the convergence between the South America upper plate, and the Nazca lower plate, where the shortening in the upper plate decreases the amount of subduction rate (Doglioni et al., 2007). The steady state shortening recorded by GPS in the orogeny possibly corresponds to creep in the ductile lower portion of the crust, and stick-slip in the brittle upper crust, which undergoes interseismic compression. In contrast, the Maule event produced approximately 3 m of westward coseismic displacement (Delouis et al., 2010), which represents the elastic rebound of the shortening accumulated during the interseismic period (Fig. 1) in the brittle shallower layer. Also in this case, the earthquake occurred in an area of low strain rate, adjacent to an area of high strain rate to the south, east and north (Fig. 4). The $M_w$ 6 Emilia (Italy) May 20, 2012, was a case of thrust-related earthquake that developed in an area of low strain rate (Fig. 5) as indicated by Cuffaro et al. (2010) and Riguzzi et al. (2012).

The Izmit, Turkey, August 17, 1999 earthquake along the North Anatolian strike-slip fault provides an example for strike-slip settings (Fig. 6). The North Anatolian Fault is 1600 km long and accommodates the dextral relative displacement at approximately 20–30 mm/yr along the plate boundary between Anatolia and Eurasia (McClusky et al., 2000). Creeping of the North Anatolian Fault was described by Cakir et al. (2005). The Izmit earthquake ruptured a segment of approximately 140 km long at its western termination near the Marmara Sea. The rupture propagated from west to east (Bohnhoff et al., 2008), which often occurs along this fault system (Barka, 1999). Both the hypocenters of Izmit and the
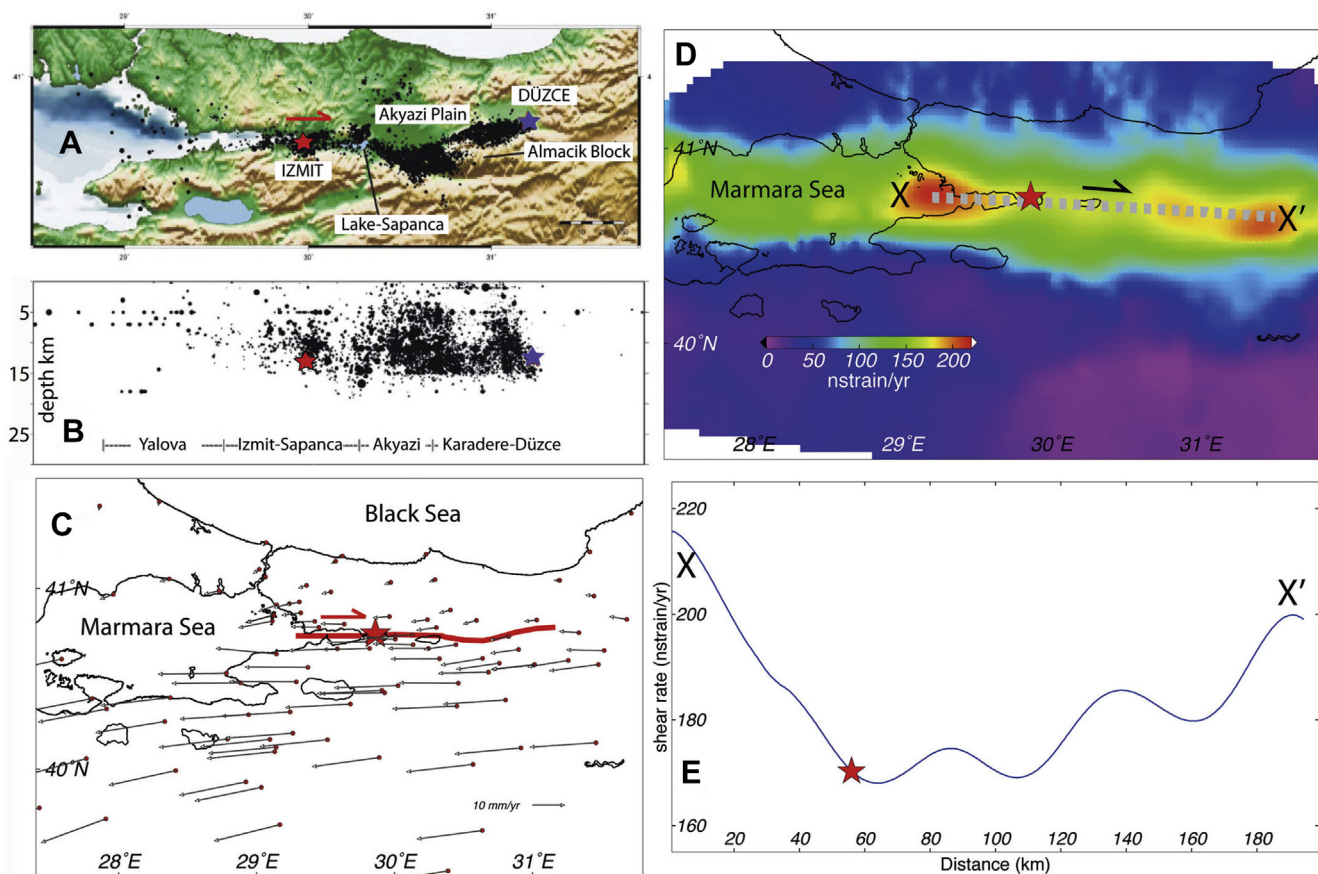


**Figure 6.** A and B: Seismicity associated to the Izmit and Düzce, Turkey, 1999 earthquakes (red and blue stars, respectively) and distribution at the depth of the events (after Bohnhoff et al., 2008). Note their upper crustal location in B. C: the pre-Izmit 1999 earthquake GPS interseismic motion relative to Eurasia, north of the North Anatolian Fault (data after Ergintav et al., 2009). The red line indicates the activated fault. D: Interseismic shear rate of the area in NW Turkey. E: Moving along the activated fault strike, the interseismic shear rate was lower where the North Anatolian fault generated the Izmit event (red star), indicating a locked or partially locked condition for that segment of the fault.
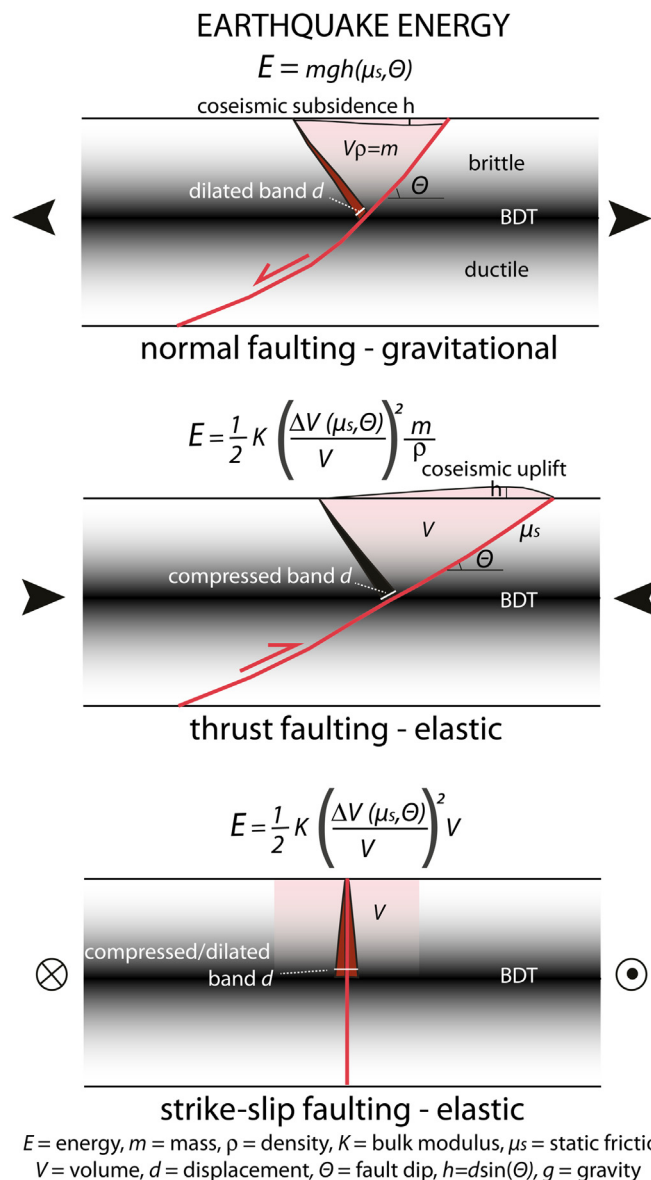
## EARTHQUAKE ENERGY

$$E = mgh(\mu_s, \Theta)$$



normal faulting - gravitational

$$E = \frac{1}{2} K \left( \frac{\Delta V (\mu_s, \Theta)}{V} \right)^2 \frac{m}{\rho}$$

thrust faulting - elastic

$$E = \frac{1}{2} K \left( \frac{\Delta V (\mu_s, \Theta)}{V} \right)^2 V$$

strike-slip faulting - elastic

$E$ = energy, $m$ = mass, $\rho$ = density, $K$ = bulk modulus, $\mu_s$ = static friction
$V$ = volume, $d$ = displacement, $\Theta$ = fault dip, $h = d\sin(\Theta)$, $g$ = gravity

**Figure 7.** The energy accumulated during the interseismic period above the BDT differs as a function of the tectonic setting. Along a normal fault, it is mostly gravitational potential energy. There probably is some elastic component but it is here assumed secondary. In contractional and strike-slip settings, it is rather elastic potential energy. The available energy is dissipated in seismic waves, friction, internal strain. The dip of the faults ($\Theta$) also controls how the energy is accumulated and released. $d$ depends on $\mu$, and $h$ on $\Theta$.

following (87 days later) Düzce earthquakes were approximately 13 km deep. Most of the aftershocks were restricted to the upper crust (5–15 km depth), suggesting the presence of a ductile, seismically silent, lower crust. The average coseismic fault slip, measured after the Izmit mainshock, ranged between 2.5 m (e.g., Tibi et al., 2001) and 2.9 m (Bouchon et al., 2002), but locally it was as large as 5–6 m (Barka et al., 2002; Bouchon et al., 2002). The pre-Izmit earthquake interseismic rates were slower along the segment of the fault later activated during the event (see data in Ergintav et al., 2009), confirming that the fault ruptured along the segment that was locked or moving slower than the adjacent segments (Fig. 6). As in the other tectonic settings, the segment along an active strike-slip fault is more prone to generate an earthquake when the interseismic strain rate is lower. However, apart a segment of the San Andreas Fault, most of the strike-slip faults do not seem to creep at all. The North Anatolian Fault has been interpreted to accumulate the same degree of strain all along the fault (Stein et al., 1997).

## 4. Energy dissipation

The fuel for earthquakes is provided by the motion of plates, where two volumes of lithosphere move at different velocity. In the contact area between the two elements energy accumulates. The elastic component is released sporadically during the earthquake. However, also gravitational energy plays a relevant role (Okamoto and Tanimoto, 2002). The seismic moment ($M_0 = \mu AD$), which expresses the energy released by an earthquake, is traditionally computed multiplying the area of the fault ($A$), the coseismic slip ($D$) and the shear modulus ($\mu$). According to the model presented here, the magnitude of the earthquake depends on the volume of the upper crust involved in the cycle, the elastic or elastoplastic parameters, the amount of dislocation, and the tectonic style. According to the aforementioned model, the dislocation should represent the non-expressed strain in the brittle crust, which was rather accumulated in a steady-state regime in the lower ductile crust during the previous interseismic period. Starting from the

geological model, we suggest that, with a given dislocation and involved volume, each tectonic setting has its own pre-earthquake energy type. Along normal faults, the energy for the earthquake is supplied by the gravitational potential, whereas, in thrust and strike-slip faults, the energy is rather accumulated under elastic potential (Fig. 7). The elastic component accumulated during the interseismic period (e.g., *d* in Fig. 7) should be related to the coseismic displacement *h*.

Energy dissipation has a number of issues which are common to all earthquakes, such as the energy released by seismic waves, the internal strain, the work in favor of or against gravity, the friction and related shear heating along the fault, the work of fault propagation (e.g., Cooke and Murphy, 2004). Along faults where the motion is down- or up-dip, the energy dissipation also depends on the fault dip. For example, the available energy along a normal fault is given by the gravitational potential energy *mgh*, where *m* is the mass (volume×density), *g* the acceleration of gravity, and *h* the potential subsidence of the hangingwall during the coseismic slip. Assuming null friction on a vertical normal fault plane, *mgh* represents the full energy (i.e., 1) deliverable by the fall of the hangingwall. By contrast, the energy is zero if the normal fault plane is horizontal. This could explain why low-angle normal faults do not generate high magnitude earthquakes (e.g., Jackson and White, 1989; Axen, 1999; Collettini, 2011 and references therein), since during the coseismic stage the vertical component of fall is smaller than in steeper faults. Therefore, normal faults are dominated by gravitational potential energy (Doglioni et al., 2011; Dempsey et al., 2012). It can be expressed by $mgh(\mu s, \Theta) + 1/2Kd^2$ where *m* is the mass, *g* the gravity acceleration, *h* the vertical coseismic dislocation which is function of the interseismic displacement *d*, *μs* the static friction, $\Theta$ the fault dip, and *K* the elastic parameter of the rocks (Fig. 7). The elastic component of the formula in tensional tectonic settings is probably the least factor, when compared with the gravitational potential energy, because rocks under tension break with very-low shear stress. Once broken, the elastic potential energy is lost.

In contractional settings, the stress and energy distribution is different. Rocks, when deformed under compression, are characterized by yield stresses about 10 times larger than yield stresses in tensional stress fields. In addition, they can store a much larger amount of elastic energy. In fact for rocks $k_c \gg k_t$, where $k_c$ is the elasticity in contractional settings, and $k_t$ the elasticity in tensional settings. Moreover, with a given friction, moving rocks along a thrust fault needs more energy as the fault becomes steeper, since the hangingwall moves against gravity. Therefore, in this case, the energy dissipation is mostly elastic (Fig. 7).

In strike-slip settings, the dominant energy comes from the elastic potential, and in case of pure horizontal movement along equipotential gravity, no gravitational energy is dissipated, nor work done against gravity. The accuracy of the energy magnitude computation in an earthquake may depend on the adopted radiation coefficient (Choy and Boatwright, 1995). According to an earlier attempt of energy evaluation, the radiation coefficient could be higher than what expected (Doglioni et al., 2011). What presented here has certainly to be improved. However, it seems quite clear that extension, contraction and transcurrent tectonics accumulate different types of potential energy, which is eventually dissipated during the quake. Therefore, they may be showing different types of pre-seismic precursors of the imminent release of energy.

## 5. Conclusions

We analyzed the strain rate prior to seismic events in the extensional, contractional and strike-slip tectonic settings. In all the three cases, the earthquake occurred along the fault segment with the highest strain rate gradient, but it nucleated where the strain rate was lower. In our model, the bands of dilation or contraction in the deforming hangingwall develops from the BDT upward. In all cases, the BDT was relevant in controlling fault activation, ultimately determining the seismic cycle. In the interseismic stage, we assumed a constant slip rate in the ductile fault segment (shear zone), whereas the upper brittle segment is practically locked. The coseismic stage represents the rupture of the brittle layer and leads to the afterslip and postseismic stages, during which the deformation rate typically decreases with time (Marone et al., 1991). The volume of rock above the slipping ductile fault segment acts as an accumulator of elastic energy during the interseismic period. Once the shear stress has exceeded the fault strength, the mainshock occurs, and the elastic layer releases the accumulated energy (Fig. 7). From this model, the following main conclusions were drawn:

1) The volume deformed above the BDT during the interseismic stage in the upper crust and the tectonic style control the energy released by the earthquake.
2) Owing to the locked status of the brittle portion of the fault, a low value of the interseismic strain rate indicates the active faults more prone to the larger rupture and the higher magnitude (Riguzzi et al., 2012, 2013).
3) The stress distribution generated at the BDT during the interseismic period yields (a) dilation (crack opening and increase of secondary porosity) at the base of locked normal faults and (b) contraction (crack closure and decrease of secondary porosity) at the base of locked thrusts.
4) In the coseismic stage of strike-slip faulting (Fig. 1), the motion reversed along the two subvertical bands located at the fault tips, which were already deformed during the interseismic stage (i.e., the band in tension experienced coseismic compression, and the band in compression experienced coseismic tension).
5) The seismic cycle consists in a long period of stress loading and a rapid release of energy, which is accumulated in a different way depending on the tectonic style (mostly gravitational for normal faults, mostly elastic for thrust or reverse faults and strike-slip faults).

The lithostatic load above the BDT represents $\sigma_1$ for a normal fault, and $\sigma_3$ for a thrust. Therefore, the increase of crustal thickness and topography above the BDT favors the nucleation of normal fault-related earthquakes. Viceversa, low topography and thinner crustal thickness above the BDT facilitate thrust-related earthquakes (Carminati et al., 2004; Doglioni et al., 2011). Our model and the supporting evidence suggest that the combination of tectonic setting, GPS, strain rate transients can help to develop a physical basis for time-dependent earthquake hazard studies. Earthquake occurrence cannot be predicted with sufficient accuracy yet. Unlike meteorological forecasts, the parameters determining an earthquake are much more complex and, unfortunately, much less measurable so far. However, progresses are continuously advancing (e.g., Peresan et al., 2005; Panza et al., 2012), and a roadmap for earthquake forecasting is possible, but we need a multiparametric approach and a more diffuse monitoring along active faults. Statistical-probabilistic studies should be accompanied by geological, seismological and space geodesy researches, which may help determine where next large earthquakes could develop in the mid-term. In a companion paper (Doglioni et al., 2013), we propose the fluids behavior as a further complementary parameter, which may help to infer short-term seismic events. However, even if the low strain rates may indicate active fault planes more prone to generate larger seismicity regardless the tectonic setting, precursors

phenomena should rather be different as a function of the tectonic style and the type of accumulated energy.

## Acknowledgments

## References

Anzidei, M., Boschi, E., Cannelli, V., Devoti, R., Esposito, A., Galvani, A., Melini, D., Pietrantonio, G., Riguzzi, F., Sepe, V., Serpelloni, E., 2009. Coseismic deformation of the destructive April 6, 2009 L'Aquila earthquake (central Italy) from GPS data. Geophysical Research Letters 36, L17307. http://dx.doi.org/10.1029/2009GL039145.

Atzori, S., Hunstad, I., Chini, M., Salvi, S., Tolomei, C., Bignami, C., Stramondo, S., Trasatti, E., Antonioli, A., Boschi, E., 2009. Finite fault inversion of DInSAR coseismic displacement of the 2009 L'Aquila earthquake (central Italy). Geophysical Research Letters 36, L15305. http://dx.doi.org/10.1029/2009GL039293.

Axen, G.J., 1999. Low-angle normal fault earthquakes and triggering. Geophysical Research Letters 26, 3693−3696. http://dx.doi.org/10.1029/1999GL005405.

Barka, A., 1999. The 17 August Izmit earthquake. Science 285, 1858−1859.

Barka, A., Akyuz, H.S., Altunel, E., et al., 2002. The surface rupture and slip distribution of the 17 August 1999 Izmit earthquake (M 7.4), North Anatolian fault. Bulletin Seismological Society of America 92 (1), 43−60.

Bernoulli, D., 1964. Zur Geologie des Monte Generoso (Lombardische Alpen): Beitr. Geol. Karte Schweiz N.F, vol. 118, pp. 1−134.

Bertotti, G., Siletto, G.B., Spalla, M.I., 1993. Deformation and metamorphism associated with crustal rifting: the Permian to Liassic evolution of the Lake Lugano-Lake Como area (Southern Alps). Tectonophysics 226, 271−284.

Bohnhoff, M., Bulut, F., Görgün, E., Milkereit, C., Dresen, G., 2008. Seismotectonic setting at the North Anatolian Fault Zone after the 1999 Mw = 7.4 Izmit earthquake based on high-resolution aftershock locations. Advances in Geosciences 14, 85−92.

Bouchon, M., Töksöz, M.N., Karabulut, H., Bouin, M.-P., Dietrich, M., Aktar, M., Edie, M., 2002. Space and time evolution of rupture and faulting during the 1999 Izmit (Turkey) earthquake. Bulletin Seismological Society of America 92 (1), 256−266.

Brooks, B., Foster, J., Bevis, M., Smalley, B., Parra, H., Baez Soto, J.C., Blanco, M., Kendrick, E., Genrich, J., Caccamise, D., 2010. Interseismic and Cosismic GPS Velocities of the Maule Mw 8.8 Chile, February 27, 2010, Earthquake. http://supersites.earthobservations.org/chile.php#Thurs5.

Burrato, F., Ciucci, F., Valensise, G., 2003. An inventory of river anomalies in the Po Plain, Northern Italy: evidence for active blind thrust faulting. Annals of Geophysics 46 (5), 865−882.

Carafa, M.M.C., Barba, S., 2011. Determining rheology from deformation data: the case of central Italy. Tectonics 30, TC2003. http://dx.doi.org/10.1029/2010TC002680.

Cakir, Z., Akoglu, A.M., Belabbes, S., Ergintav, S., Meghraoui, M., 2005. Creeping along the Ismetpasa section of the North Anatolian fault (Western Turkey): rate and extent from InSAR convection. Earth and Planetary Science Letters 238, 225−234. http://dx.doi.org/10.1016/j.epsl.2005.06.044.

Carminati, E., Doglioni, C., Barba, S., 2004. Reverse migration of seismicity on thrusts and normal faults. Earth Science Reviews 65, 195−222.

Cattin, R., Avouac, J.P., 2000. Modeling mountain building and the seismic cycle in the Himalaya of Nepal. Journal of Geophysical Research 105 (B6), 13,389−13,407.

Chiarabba, C., 28 others, 2009. The 2009 L'Aquila (central Italy) MW6.3 earthquake: main shock and aftershocks. Geophysical Research Letters 36, L18308. http://dx.doi.org/10.1029/2009GL039627.

Chiarabba, C., Jovane, L., Di Stefano, R., 2005. A new view of Italian seismicity using 20 years of instrumental recordings. Tectonophysics 395, 251−268.

Choy, G.L., Boatwright, J.L., 1995. Global patterns of radiated seismic energy and apparent stress. Journal of Geophysical Research 100 (B9), 18205−18228. http://dx.doi.org/10.1029/95JB01969.

Collettini, C., 2011. The mechanical paradox of low-angle normal faults: current understanding and open questions. Tectonophysics 510, 253−268. http://dx.doi.org/10.1016/j.tecto.2011.07.015.

Cooke, M.L., Murphy, S., 2004. Assessing the work budget and efficiency of fault systems using mechanical models. Journal of Geophysical Research 109, B10408. http://dx.doi.org/10.1029/2004JB002968.

Cuffaro, M., Riguzzi, F., Scrocca, D., Antonioli, F., Carminati, E., Livani, M., Doglioni, C., 2010. On the geodynamics of the northern Adriatic plate. Rendiconti Lincei 21 (Suppl. 1), S253−S279. http://dx.doi.org/10.1007/s12210-010-0098-9.

Delouis, B., Nocquet, J.-M., Vallée, M., 2010. Slip distribution of the February 27, 2010 Mw = 8.8 Maule Earthquake, central Chile, from static and high-rate GPS, InSAR, and broadband teleseismic data. Geophysical Research Letters 37, L17305. http://dx.doi.org/10.1029/2010GL043899.

Dempsey, D., Ellis, S., Archer, R., Rowland, J., 2012. Energetics of normal earthquakes on dip-slip faults. Geology 40, 279−282.

Devoti, R., Riguzzi, F., Cuffaro, M., Doglioni, C., 2008. New GPS constraints on the kinematics of the Apennine subduction. Earth and Planetary Science Letters 273 (1−2), 163−174.

Devoti, R., Esposito, A., Pietrantonio, G., Pisani, A.R., Riguzzi, F., 2011. Evidence of large scale deformation patterns from GPS data in the Italian subduction boundary. Earth and Planetary Science Letters 311, 230−241.

Di Luccio, F., Ventura, G., Di Giovambattista, R., Piscini, A., Cinti, F.R., 2010. Normal faults and thrusts re-activated by deep fluids: the 6 April 2009 Mw 6.3 L'Aquila earthquake, central Italy. Journal of Geophysical Research 115 (B06315), 15. http://dx.doi.org/10.1029/2009JB007190.

Doglioni, C., Barba, S., Carminati, E., Riguzzi, F., 2011. Role of the brittle-ductile transition on fault activation. Physics of the Earth and Planetary Interiors 184, 160−171. http://dx.doi.org/10.1016/j.pepi.2010.11.005.

Doglioni, C., Barba, S., Carminati, E., Riguzzi, F., 2013. Fault on-off versus coseismic fluids reaction. Geoscience Frontiers. http://dx.doi.org/10.1016/j.gsf.2013.08.004.

Doglioni, C., Carminati, E., Cuffaro, M., Scrocca, D., 2007. Subduction kinematics and dynamic constraints. Earth Science Reviews 83, 125−175. http://dx.doi.org/10.1016/j.earscirev.2007.04.001.

Dragert, H., Wang, K., James, T.S., 2001. A silent slip event on the deeper Cascadia subduction interface. Science 292 (5521), 1525−1528. http://dx.doi.org/10.1126/science.1060152.

EMERGEO Working Group, 2010. Evidence for surface rupture associated with the Mw 6.3 L'Aquila earthquake sequence of April 2009 (central Italy). Terra Nova 22, 43−51.

Ergintav, S., McClusky, S., Hearn, E., Reilinger, R., Cakmak, R., Herring, T., Ozener, H., Lenk, O., Tari, E., 2009. Seven years of postseismic deformation following the 1999, M = 7.4 and M = 7.2, Izmit-Düzce, Turkey earthquake sequence. Journal of Geophysical Research 114, B07403. http://dx.doi.org/10.1029/2008JB006021.

Feigl, K.L., Thatcher, W., 2006. Geodetic observations of post-seismic transients in the context of the earthquake deformation cycle. Comptes Rendus Geosciences, 'Observing the Earth from space' 338, 1012−1028.

Frank, F.C., 1965. On dilatancy in relation to seismic sources. Reviews of Geophysics 3, 485−503.

Galli, P., Giaccio, B., Messina, P., 2010. The 2009 central Italy earthquake seen through 0.5 Myr-long tectonic history of the L'Aquila faults system. Quaternary Science Reviews 29 (27−28), 3768−3789.

Hetland, E.A., Simons, M., Dunham, E., 2010. Post-seismic and interseismic fault creep I: model description. Geophysical Journal International 181, 81−98. http://dx.doi.org/10.1111/j.1365-246X.2010.04522.x.

Hobbs, B., Ord, A., 1988. Plastic instabilities: Implications for the origin of intermediate and deep focus earthquakes. Journal of Geophysical Research 93 (B9). http://dx.doi.org/10.1029/JB093iB09p10521.

Jackson, J.A., White, N.J., 1989. Normal faulting in the upper continental crust: observations from regions of active extension. Journal of Structural Geology 11, 15−36.

Kanamori, H., Anderson, D.L., 1975. Theoretical basis of some empirical relations in seismology. Bulletin of Seismological Society of America 65, 1073−1095.

Klinger, Y., Avouac, J.P., Dorbath, L., Abou Karaki, N., Tisnerat, N., 2000. Seismic behaviour of the Dead Sea fault along Araba valley, Jordan. Geophysical Journal International 142, 769−782.

Lin, W., Conin, Marianne, Moore, J. Casey, Chester, Frederick M., Nakamura, Yasuyuki, Mori, James J., Anderson, Louise, Brodsky, Emily E., Eguchi, Nobuhisa, Expedition 343 Scientists, 2013. Stress state in the Largest displacement area of the 2011, Tohoku-Oki earthquake. Science 339, 687−690.

Liu, M., Yang, Y., Stein, S., Zhu, Y., Engeln, J., 2000. Crustal shortening in the Andes: why do GPS rates differ from geological rates? Geophysical Research Letters 27, 3005−3008.

Marone, C.J., Scholtz, C.H., Bilham, R., 1991. On the mechanics of earthquake afterslip. Journal of Geophysical Research 96 (B5), 8441−8452.

Marone, C., 1998. Laboratory-derived friction laws and their application to seismic faulting. Annual Review of Earth Planetary Science 26, 643−696.

Massonnet, D., Rossi, M., Carmona, C., Adragna, F., Peltzer, G., Fiegl, K., Rabaute, T., 1993. The displacement field of the Landers earthquake mapped by radar interferometry. Nature 364, 138−142.

McClusky, S., Balassanian, S., Barka, A., et al., 2000. Global positioning system constraints on plate kinematics and dynamics in the eastern Mediterranean and Caucasus. Journal of Geophysical Research 105, 5695−5719.

Meade, B.J., Hager, B.H., 2005. Block models of crustal motion in southern California constrained by GPS measurements. Journal of Geophysical Research 110, B03403. http://dx.doi.org/10.1029/2004JB003209.

Meltzner, A.J., Sieh, K., Abrams, M., Agnew, D.C., Hudnut, K.W., Avouac, J.-P., Natawidjaja, D., 2006. Uplift and subsidence associated with the great Aceh-Andaman earthquake of 2004. Journal of Geophysical Research 111, B02407. http://dx.doi.org/10.1029/2005JB003891.

Moreno, M., Rosenau, M., Oncken, O., 2010. Maule earthquake slip correlates with pre-seismic locking of Andean subduction zone. Nature 467, 198−202.

Nuchter, J.A., Stockhert, B., 2008. Coupled stress and pore fluid pressure changes in the middle crust: vein record of coseismic loading and postseismic stress relaxation. Tectonics 27, TC1007. http://dx.doi.org/10.1029/2007TC002180.

Okada, Y., 1992. Internal deformation due to shear and tensile faults in a half-space. Bulletin Seismological Society of America, 1018–1040.

Okamoto, T., Tanimoto, T., 2002. Crustal gravitational energy change caused by earthquakes in the western United States and Japan. Earth and Planetary Science Letters 195, 17–27.

Panza, G.F., La Mura, C., Peresan, A., Romanelli, F., Vaccari, F., 2012. Seismic hazard scenarios as preventive tools for a disaster resilient society. In: Dmowska, R. (Ed.), Advances in Geophysics. Elsevier, London, pp. 93–165.

Peresan, A., Kossobokov, V., Romashkova, L., Panza, G.F., 2005. Intermediate-term middle-range earthquake predictions in Italy: a review. Earth Science Reviews 69, 97–132.

Pieri, M., 1983. Three seismic profiles through the Po Plain. In: Bally, A.W. (Ed.), Seismic Expression of Structural Styles, AAPG Studies in Geology, vol. 15(3), pp. 3.4.1–3.4.8.

Pingue, F., De Natale, G., 1993. Fault mechanism of the 40 seconds subevent of the 1980 Irpinia (Southern Italy) earthquake from levelling data. Geophysical Research Letters 20 (10), 911–914.

Prawirodirdjo, L., McCaffrey, R., Chadwell, C.D., Bock, Y., Subarya, C., 2010. Geodetic observations of an earthquake cycle at the Sumatra subduction zone: role of interseismic strain segmentation. Journal of Geophysical Research 115, B03414. http://dx.doi.org/10.1029/2008JB006139.

Riguzzi, F., Crespi, M., Devoti, R., Doglioni, C., Pietrantonio, G., Pisani, A.R., 2012. Geodetic strain rate and earthquake size: new clues for seismic hazard studies. Physics of the Earth and Planetary Interiors 206–207, 67–75.

Riguzzi, F., Crespi, M., Devoti, R., Doglioni, C., Pietrantonio, G., Pisani, A.R., 2013. Strain rate relaxation of normal and thrust faults in Italy. Geophysical Journal International 195, 815–820. http://dx.doi.org/10.1093/gji/ggt304.

Rosen, P., Werner, C., Fielding, E., Hensley, S., Buckley, S., Vincent, P., 1998. Aseismic creep along the San Andreas Fault northwest of Parkfield, CA measured by radar interferometry. Geophysical Research Letters 25 (6), 825–828.

Ruegg, J.C., Rudloff, A., Vigny, C., Madariaga, R., de Chabalier, J.B., Campos, J., Kausel, E., Barrientos, S., Dimitrov, D., 2009. Interseismic strain accumulation measured by GPS in the seismic gap between Constitución and Concepción in Chile. Physics of the Earth and Planetary Interiors 175, 78–85. http://dx.doi.org/10.1016/j.pepi.2008.02.015.

Ruina, A., 1983. Slip instability and state variable friction laws. Journal of Geophysical Research 88, 10359–10370.

Savage, J.C., 1983. A dislocation model of strain accumulation and release at a subduction zone. Journal of Geophysical Research 88, 4984–4996.

Savage, J.C., Burford, R.O., 1973. Geodetic determination of relative plate motion in central California. Journal of Geophysical Research 78, 832–845.

Savage, J.C., Prescott, W.H., 1978. Asthenosphere readjustment and the earthquake cycle. Journal of Geophysical Research 83, 3369–3376.

Schleicher, A.M., van der Pluijm, B.A., Warr, L.N., 2010. Nanocoatings of clay and creep of the San Andreas fault at Parkfield, California. Geology 38 (7), 667–670. http://dx.doi.org/10.1130/G31091.1.

Scholz, C.H., 1990. The Mechanics of Earthquakes and Faulting. Cambridge University Press, Cambridge, New York. Ref. QE534.2.S37.

Shen, Z.K., Jackson, D.D., Ge, B.X., 1996. Crustal deformation across and beyond the Los Angeles basin from geodetic measurements. Journal of Geophysical Research 101, 27,957–27,980.

Shen, Z.-K., Jackson, D.D., Kagan, Y.Y., 2007. Implications of geodetic strain rate for future earthquakes, with a five-year forecast of M5 earthquakes in Southern California. Seismological Research Letters 78, 116–120.

Sibson, R.H., 1977. Faults rocks and fault mechanisms. Journal of the Geology Society London 133, 191–213.

Sieh, K., Natawidjaja, D.H., Meltzner, A.J., Shen, C.-C., Cheng, H., Li, K.-S., Suwargadi, B.W., Galetzka, J., Philibosian, B., Edwards, R.L., 2008. Earthquake supercycles inferred from sea-level changes recorded in the Corals of West Sumatra. Science 322 (5908), 1674–1678. http://dx.doi.org/10.1126/science.1163589.

Sladen, A., 2010. http://www.tectonics.caltech.edu/slip_history/2010_chile/index.html.

Stein, R.S., Barka, A.A., Dieterich, J.H., 1997. Progressive failure on the North Anatolian fault since 1939 by earthquake stress triggering. Geophysical Journal International 128, 594–604.

Thatcher, W., Rundle, J.B., 1979. A model for the earthquake cycle in underthrust zones. Journal of Geophysical Research 84, 5540–5556.

Tibi, R., Bock, G., Xia, Y., Baumbach, M., Grosser, H., Milkereit, C., Karakisa, S., Zünbul, S., Kind, R., Zschau, J., 2001. Rupture processes of the 1999 August 17 Izmit and November 12 Düzce (Turkey) earthquakes. Geophysical Journal International 144, F1–F7.

Vezzani, L., Ghisetti, F., 1998. Carta Geologica dell'Abruzzo, scala 1/100.000. Regione Abruzzo. Selca.